Available online at www.sciencedirect.com
ScienceDirect
Journal of Sound and Vibration 313 (2008) 723–737
JOURNAL OF SOUND AND VIBRATION
www.elsevier.com/locate/jsvi

Acoustic power in non-uniform lined ducts ☆

Walter Eversman

Mechanical and Aerospace Engineering, University of Missouri-Rolla, Rolla, MO 65401, USA

Handling Editor: C. Morfey
Available online 14 March 2008

Abstract

A definition of acoustic power in conservation form in lined infinitely long uniform ducts is extended to include axially symmetric non-uniform ducts with potential mean flow and finite length lining. The definition includes a contribution at the lined boundary. Benchmarking is accomplished by verification of acoustic power conservation in the case of a purely reactive lining. Calculations in the case of reactively lined ducts show that intense acoustic gradients near the lined surface can occur, and contributions to acoustic power from the boundary power term become relatively large. This observed behavior diminishes as the resistive component of lining impedance is increased. Power calculations for propagation and radiation from a typical turbofan inlet and equivalent calculations for an infinite duct propagation model of the same inlet contour are compared. Results are remarkably similar for the case considered, though it is noted that this conclusion is geometry dependent.

1. Introduction

Acoustic power is a convenient metric for quantification of performance of acoustic treatment in ducts. When there is no flow in the duct, the calculation of acoustic intensity and power is straightforward [1]. When steady uniform mean flow is present in a uniform duct, acoustic intensity is given in a form attributed to Ryshov and Shefter [2]. For propagation in potential mean flows in non-uniform ducts, a relationship for intensity due to Morfey [3] is applicable. Candel [4] has reviewed much of the literature pertaining to energy relationships in acoustics and identifies the Ryshov and Shefter and Morfey formulations as distinct approaches. In the common case of uniform flow in uniform ducts, the Morfey and Ryshov and Shefter representations for acoustic intensity do not match. Eversman [5] has identified how the two approaches correspond to different, but equivalent variational formulations. Other definitions of acoustic intensity have been given by Moehring for sheared flows [6] and by Godin for more general flows [7].

Eversman [5] derived acoustic power conservation relationships for the Ryshov and Shefter and Morfey intensity formulations in the case of uniform flow in a uniform duct that show that the axial gradient of acoustic power in a uniform lined duct is simply obtained in either formulation in terms of the resistance of the lining and the normal velocity of the lining. Furthermore, it was shown that a proper accounting of acoustic power includes a contribution at the wall, which is in addition to the integrated intensity across the duct

☆ Originally presented as Acoustic Power in Lined Ducts at the 10th AIAA/CEAS Aeroacoustics Conference, Manchester, England, May 10–12, 2004 Copyright 2004 by Walter Eversman.

E-mail address: eversman@umr.edu

0022-460X/$ - see front matter © 2007 Elsevier Ltd. All rights reserved.
doi:10.1016/j.jsv.2007.11.028

obtained from Ryshov and Shefter and Morfey formulations. Calculations were made to support these conclusions based on acoustic duct modes in two-dimensional ducts. All conclusions were based on a uniform duct of infinite length. The important case of a finite length lining was not considered.

The work reported here begins with an extension of the results of Eversman [5] to calculation of acoustic power according to the Morfey formulation (used exclusively because additional results reported for non-uniform ducts are limited to this formulation) in circular uniform ducts. With calculated acoustic modes in lined ducts acoustic power is obtained, including the boundary contribution. It is shown that the axial gradient of acoustic power (calculated directly from the formulation for power) matches the simple result for this gradient based only on the lining resistance and normal surface velocity at the lining. It is found that in some cases the boundary power is large and is an essential contribution to the total acoustic power.

Finite element models (FEM) of duct propagation and radiation for axially symmetric ducts provide the means to calculate intensity and power at the source and at locations along the duct and in the far field. In the work reported here, the Morfey formulation for acoustic intensity augmented by Eversman's appended boundary power is used to post-process FEM calculations for acoustic potential in non-uniform and uniform ducts carrying potential flow to numerically examine the conservation law. In the first instance, the case of a finite lining imbedded in a uniform duct with reflection free terminations (infinite duct) is considered. The most telling case occurs when the lining is purely reactive and acoustic power must be conserved. It is found numerically that acoustic power is indeed conserved for propagation from an initially unlined section, through the treated section, into an unlined exit section. This result is also obtained in the case of a non-uniform duct.

In the case of reactively lined ducts an interesting phenomenon is found. In some cases, the power in the interior of the duct in the lined section (obtained from integration of the Morfey power across the duct) is directed toward the source. The requirement for net power to be directed away from the source and to be conserved at any duct cross-section is met by acoustic power at the boundary larger in magnitude than the interior power and directed away from the source. The sum of the boundary power and interior power is directed away from the source and conserved, but boundary power and interior power individually vary significantly with axial location.

Finally, FEM calculations have been made for a typical turbo-fan inlet geometry. In one case, the duct has been modeled with a non-reflecting termination, and in a second case it has been modeled to include radiation to the far field. For conditions, which are identical, except for unavoidable differences in details of the mean flow, demonstration calculations show that conclusions drawn for lining performance based on acoustic power attenuation are similar.

2. Acoustic power

In dimensional form, acoustic energy density e (energy per unit volume) and energy flux $\vec{N}$ (instantaneous power per unit area) for irrotational acoustic perturbations on a potential steady mean flow in a hard wall duct are given by [3]

$$e = \frac{1}{2}\frac{1}{\rho_l c_l^2}p^2 + \frac{1}{2}\rho_l \vec{v}\cdot\vec{v} + \frac{1}{c_l^2}(\vec{V}_0\cdot\vec{v})p \tag{1}$$

and

$$\vec{N} = p\vec{v} + \frac{1}{\rho_l c_l^2}\vec{V}_0 p^2 + \rho_l(\vec{V}_0\cdot\vec{v})\vec{v} + \frac{1}{c_l^2}\vec{V}_0(\vec{V}_0\cdot\vec{v})p. \tag{2}$$

$\vec{V}_0$, ρ_l, c_l are local mean flow velocity, density, and speed of sound. $p, \vec{v}$ are acoustic pressure and particle velocity. Energy density and energy flux are related by the conservation law

$$\frac{\partial e}{\partial t} + \operatorname{div}\vec{N} = 0. \tag{3}$$

Consider a section of non-uniform duct of volume V enclosed by a surface S shown in Fig. 1. Following the approach of Eversman [5], assume there is a section of the duct wall on which a locally reacting lining exists. The lining is modeled with kinetic and potential energy per unit area T and U at the boundary with input

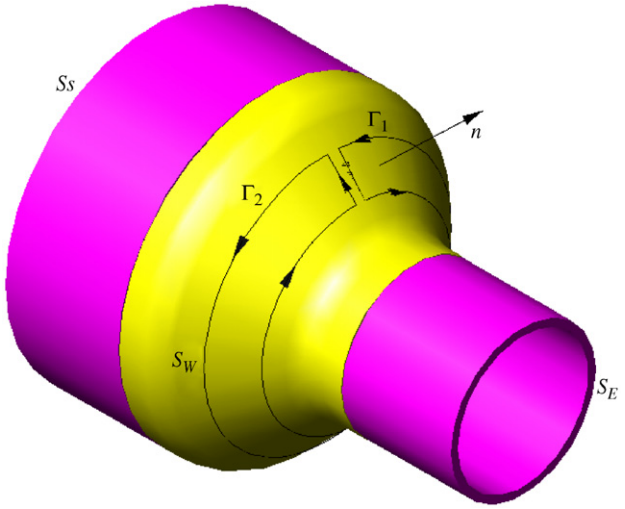

Fig. 1. General view of a segment of an axi-symmetric duct bounded by cross-sections S_s and S_E and duct wall S_W. $\vec{n}$ is the unit outward normal. Γ_1 and Γ_2 are closed contours on the duct surface S_W. The light area represents the lining location.

power per unit area due to acoustic pressure and boundary resistance proportional to boundary normal velocity. On the wall surface S_w the power balance is

$$\iint_{S_w} \frac{\partial}{\partial t}(T+U)\,\mathrm{d}S = \iint_{S_w} (p\zeta_t - r_b\zeta_t^2)\,\mathrm{d}S. \tag{4}$$

ζ is the displacement of the impedance surface normal to the undeformed surface.

This would be consistent with the common single-degree-of-freedom oscillator lining model with parameters m_b, r_b, k_b (per unit area) according to

$$m_b\zeta_{tt} + r_b\zeta_t + k_b\zeta = p. \tag{5}$$

In the harmonic case (frequency ω), this yields the impedance relation

$$\frac{p}{\zeta_t} = Z = r(\omega) + \mathrm{i}\chi(\omega) = r_b + \mathrm{i}\left(\omega m_b - \frac{k_b}{\omega}\right). \tag{6}$$

The power formulation of Eq. (4) allows a more general linear lining model, for example two degrees of freedom, with a more complicated impedance.

The total energy for the duct and lining enclosed by S is for the general case and for the single-degree-of-freedom analog

$$E = \iiint_V e\,\mathrm{d}V + \iint_{S_W}(T+U)\,\mathrm{d}S = \iiint_V e\,\mathrm{d}V + \iint_{S_W}\frac{1}{2}m_b\zeta_t^2\,\mathrm{d}S + \iint_{S_W}\frac{1}{2}k_b\zeta^2\,\mathrm{d}S. \tag{7}$$

S_w denotes that portion of S that includes the duct walls and lining. By making use of the energy conservation law (3) and the lining models of Eqs. (4) or (5) it is easily shown that

$$\frac{\partial E}{\partial t} = -\iiint_V \mathrm{div}\,\vec{N}\,\mathrm{d}V + \iint_{S_W} p\zeta_t\,\mathrm{d}S - \iint_{S_W} r_b\zeta_t^2\,\mathrm{d}S. \tag{8}$$

For steady harmonic excitation, it follows that the time average of the rate of change of acoustic energy in V vanishes, that is $\langle \partial E/\partial t\rangle = 0$, so that

$$\iiint_V \mathrm{div}\left\langle \vec{N}\right\rangle \mathrm{d}V - \iint_{S_W}\langle p\zeta_t\rangle\,\mathrm{d}S = -\iint_{S_W} r_b\langle\zeta_t^2\rangle\,\mathrm{d}S. \tag{9}$$

With use of the divergence theorem Eq. (9) reduces to surface integrals over the total area S, enclosing the volume V, and the wall area S_w,

$$\iint_S \left\langle \vec{N}\cdot\vec{n}\right\rangle \mathrm{d}S - \iint_{S_W}\langle p\zeta_t\rangle\,\mathrm{d}S = -\iint_{S_W} r_b\langle\zeta_t^2\rangle\,\mathrm{d}S. \tag{10}$$

Now in Fig. 1 consider the duct segment to be infinitesimal of length Δx. At $x = x_s$, the duct is bounded by the cross-sectional surface S_s with normal $\vec{n} = -\vec{i}$. At $x = x_E = x_s + \Delta x$, the duct is bounded by cross-sectional surface S_E with normal $\vec{n} = \vec{i}$. Because the normal component of mean flow vanishes on S_W only two terms of the integral over S are non-zero on S_W. Eq. (10) becomes

$$\iint_{S_E}\left\langle \vec{N}\cdot\vec{i}\right\rangle \mathrm{d}S - \iint_{S_S}\left\langle \vec{N}\cdot\vec{i}\right\rangle \mathrm{d}S + \iint_{S_w}\left[\langle p\vec{v}\cdot\vec{n}\rangle + \rho_l(\vec{V}_0\cdot\vec{v})\vec{v}\cdot\vec{n}\right]\mathrm{d}S - \iint_{S_w}\langle p\zeta_t\rangle\,\mathrm{d}S = -\iint_{S_w} r_b\langle\zeta_t^2\rangle\,\mathrm{d}S. \tag{11}$$

On S_W the normal velocity boundary condition is [8]

$$\vec{v}\cdot\vec{n} = \zeta_t + \vec{V}_0\cdot\ \mathrm{grad}\,\zeta - \zeta\vec{n}\cdot(\vec{n}\cdot\ \mathrm{grad})\vec{V}_0. \tag{12}$$

ζ_t is the velocity of the boundary in the direction normal to the undeformed boundary (the normal is directed outward).

This leads to an alternate form of Eq. (11),

$$\begin{aligned}&\iint_{S_E}\left\langle \vec{N}\cdot\vec{i}\right\rangle \mathrm{d}S - \iint_{S_S}\left\langle \vec{N}\cdot\vec{i}\right\rangle \mathrm{d}S\\ &\quad+\iint_{S_W}\left[\left\langle\left(\frac{p}{\rho_l}+\vec{V}_0\cdot\vec{v}\right)\rho_l\vec{V}_0\cdot\ \mathrm{grad}\,\zeta\right\rangle + \left\langle\rho_l(\vec{V}_0\cdot\vec{v})\zeta_t\right\rangle\right.\\ &\quad\left.-\left\langle\left(\frac{p}{\rho_l}+\vec{V}_0\cdot\vec{v}\right)\rho_l\zeta\vec{n}\cdot(\vec{n}\cdot\ \mathrm{grad}\ \vec{V}_0)\right\rangle\right]\mathrm{d}S = -\iint_{S_W} r_b\langle\zeta_t^2\rangle\,\mathrm{d}S.\end{aligned} \tag{13}$$

For steady harmonic time dependence $\langle\rho_l\vec{V}_0\cdot\partial/\partial t(\vec{v}\zeta)\rangle = 0$, leading to the result

$$\left\langle\rho_l(\vec{V}_0\cdot\vec{v})\zeta_t\right\rangle = -\left\langle\rho_l(\vec{V}_0\cdot\vec{v}_t)\zeta\right\rangle. \tag{14}$$

The acoustic momentum equation provides the relationship

$$\vec{v}_t = -\ \mathrm{grad}\left(\vec{V}_0\cdot\vec{v}+\frac{p}{\rho_l}\right). \tag{15}$$

The boundary term in Eq. (13),

$$I_W = \iint_{S_W}\left[\left\langle\left(\frac{p}{\rho_l}+\vec{V}_0\cdot\vec{v}\right)\rho_l\vec{V}_0\cdot\ \mathrm{grad}\,\zeta\right\rangle + \left\langle\rho_l(\vec{V}_0\cdot\vec{v})\zeta_t\right\rangle - \left\langle\left(\frac{p}{\rho_l}+\vec{V}_0\cdot\vec{v}\right)\rho_l\zeta\vec{n}\cdot(\vec{n}\cdot\ \mathrm{grad}\ \vec{V}_0)\right\rangle\right]\mathrm{d}S, \tag{16}$$

is modified with the use of Eqs. (14) and (15) to yield

$$\begin{aligned}I_W = \iint_{S_W}&\left[\left\langle\rho_l\vec{V}_0\cdot\left(\frac{p}{\rho_l}+\vec{V}_0\cdot\vec{v}\right)\mathrm{grad}\,\zeta\right\rangle\right.\\ &\left.+\left\langle\rho_l\vec{V}_0\cdot\zeta\ \mathrm{grad}\left(\frac{p}{\rho_l}+\vec{V}_0\cdot\vec{v}\right)\right\rangle - \left\langle\rho_l\left(\frac{p}{\rho_l}+\vec{V}_0\cdot\vec{v}\right)\zeta\vec{n}\cdot(\vec{n}\cdot\ \mathrm{grad}\ \vec{V}_0)\right\rangle\right]\mathrm{d}S.\end{aligned} \tag{17}$$

This is equivalent to

$$I_W = \iint_{S_W}\left[\left\langle\rho_l\vec{V}_0\cdot\ \mathrm{grad}\left(\frac{p}{\rho_l}+\vec{V}_0\cdot\vec{v}\right)\zeta\right\rangle - \left\langle\rho_l\left(\frac{p}{\rho_l}+\vec{V}_0\cdot\vec{v}\right)\zeta\vec{n}\cdot(\vec{n}\cdot\ \mathrm{grad}\ \vec{V}_0)\right\rangle\right]\mathrm{d}S. \tag{18}$$

Since for the steady mean flow div $\rho_l \vec{V}_0 = 0$, and $\vec{V}_0 \cdot \vec{n} = 0$ on S_W, Eq. (18) further simplifies to

$$I_W = \iint_{S_W} \left[\left\langle \text{div}\, \rho_l \vec{V}_0 \left(\frac{p}{\rho_l} + \vec{V}_0 \cdot \vec{v} \right) \zeta \right\rangle - \left\langle \vec{n} \cdot (\vec{n} \cdot \text{ grad}) \rho_l \left(\frac{p}{\rho_l} + \vec{V}_0 \cdot \vec{v} \right) \zeta \vec{V}_0 \right\rangle \right] \mathrm{d}S. \tag{19}$$

A vector identity yields

$$\left\langle \vec{n} \cdot (\vec{n} \cdot \text{ grad}) \rho_l \vec{V}_0 \left(\frac{p}{\rho_l} + \vec{V}_0 \cdot \vec{v} \right) \zeta \right\rangle = \left\langle \text{div}\, \rho_l \vec{V}_0 \left(\frac{p}{\rho_l} + \vec{V}_0 \cdot \vec{v} \right) \zeta \right\rangle - \left\langle \vec{n} \cdot \text{ curl} \left[\vec{n} \times \rho_l \vec{V}_0 \left(\frac{p}{\rho_l} + \vec{V}_0 \cdot \vec{v} \right) \zeta \right] \right\rangle. \tag{20}$$

With Eq. (20), the boundary integral of Eq. (18) is greatly simplified to

$$I_W = \iint_{S_W} \left\langle \vec{n} \cdot \text{ curl}\, \vec{n} \times \rho_l \vec{V}_0 \left(\frac{p}{\rho_l} + \vec{V}_0 \cdot \vec{v} \right) \zeta \right\rangle \mathrm{d}S. \tag{21}$$

Stokes' Theorem allows the recasting of Eq. (21) as a line integral on the boundary Γ of S_W. By reference to Fig. 1, this is interpreted in terms of the contours Γ_1 and Γ_2 and the cut on which the net contribution vanishes. The result is

$$I_W = \oint_{\Gamma_1} \left\langle \vec{n} \times \rho_l \vec{V}_0 \left(\frac{p}{\rho_l} + \vec{V}_0 \cdot \vec{v} \right) \zeta \right\rangle \cdot \mathrm{d}\vec{\Gamma} + \oint_{\Gamma_2} \left\langle \vec{n} \times \rho_l \vec{V}_0 \left(\frac{p}{\rho_l} + \vec{V}_0 \cdot \vec{v} \right) \zeta \right\rangle \cdot \mathrm{d}\vec{\Gamma}. \tag{22}$$

The vector $\vec{n}$ is the outward normal to S_W. $\vec{V}_0$ is tangent to S_W with no azimuthal component. $\vec{n} \times \vec{V}_0 \cdot \mathrm{d}\vec{\Gamma}$ is then $V_0\, \mathrm{d}\Gamma$ on Γ_2 and $-V_0\, \mathrm{d}\Gamma$ on Γ_1, where V_0 is the velocity tangent to the surface S_W. Therefore,

$$I_W = \int_{\Gamma_2} \left\langle \rho_l V_0 \left(\frac{p}{\rho_l} + \vec{V}_0 \cdot \vec{v} \right) \zeta \right\rangle \mathrm{d}\Gamma - \int_{\Gamma_1} \left\langle \rho_l V_0 \left(\frac{p}{\rho_l} + \vec{V}_0 \cdot \vec{v} \right) \zeta \right\rangle \mathrm{d}\Gamma. \tag{23}$$

Returning to Eq (11), make the interpretation

$$\iint_{S_E} \left\langle \vec{N} \cdot \vec{i} \right\rangle \mathrm{d}S - \iint_{S_S} \left\langle \vec{N} \cdot \vec{i} \right\rangle \mathrm{d}S = \frac{\mathrm{d}}{\mathrm{d}x} \iint_{S_c} \left\langle \vec{N} \cdot \vec{i} \right\rangle \mathrm{d}S \Delta x = \frac{\mathrm{d}P_I}{\mathrm{d}x} \Delta x. \tag{24}$$

S_c explicitly identifies that the area is the duct cross-section. Similarly, in Eq. (23) make the interpretation

$$I_w = \frac{\mathrm{d}P_w}{\mathrm{d}x} \Delta x = \frac{\mathrm{d}}{\mathrm{d}x} \int_{\Gamma} \left\langle \rho_l V_0 \left(\frac{p}{\rho_l} + \vec{V}_0 \cdot \vec{v} \right) \zeta \right\rangle \mathrm{d}\Gamma \Delta x. \tag{25}$$

The surface integral defining dissipation is represented by

$$I_{\mathrm{d}} = \iint_{\Delta S_b} r_b \langle \zeta_t^2 \rangle \, \mathrm{d}S. \tag{26}$$

Here, the surface integral is over the incremental area ΔS_w, consistent with the incremental length Δx. Eq. (11) becomes

$$\frac{\mathrm{d}P_I}{\mathrm{d}x} + \frac{\mathrm{d}P_w}{\mathrm{d}x} = \frac{\mathrm{d}P_I}{\mathrm{d}x} + \frac{\mathrm{d}}{\mathrm{d}x} \int_{\Gamma} \left\langle \rho_l V_0 \left(\frac{p}{\rho_l} + \vec{V}_0 \cdot \vec{v} \right) \zeta \right\rangle \mathrm{d}\Gamma = - \lim_{\Delta x \to 0} \frac{1}{\Delta x} \iint_{\Delta S_w} r_b \langle \zeta_t^2 \rangle \, \mathrm{d}S, \tag{27}$$

where the interior power and boundary power are defined by

$$P_I = \iint_{S_c} \left\langle \vec{N} \cdot \vec{i} \right\rangle \mathrm{d}S, \; P_w = \int_\Gamma \left\langle \rho_l V_0 \left(\frac{p}{\rho_l} + \vec{V}_0 \cdot \vec{v} \right) \zeta \right\rangle \mathrm{d}\Gamma \tag{28}$$

with $\vec{N}$ defined by Eq. (2). A modified (total) power that includes a surface contribution is then identified as

$$P_T = P_I + \int_\Gamma \left\langle \rho_l V_0 \left(\frac{p}{\rho_l} + \vec{V}_0 \cdot \vec{v} \right) \zeta \right\rangle \mathrm{d}\Gamma. \tag{29}$$

While Fig. 1 and the development above suggest that only the outer wall of a circular duct is considered, it can easily be generalized to include an annular duct. The definition of acoustic power in a non-uniform lined duct given by Eq. (29) is a generalization of the result obtained in Ref. [5] for a two-dimensional uniform duct and reduces to it.

3. Non-dimensional power

Calculations presented in this investigation have been carried out with FEM for propagation and far-field radiation, which include FEM calculation of axial wavenumbers [9–12]. Field equations are written in non-dimensional form. Reference density and speed of sound are ρ_∞, c_∞. For an infinite duct, these conditions are at the source plane, nominally $x = 0$. For the radiating duct, reference conditions are in the far field where mean flow is uniform [9]. A reference length R is defined by the duct radius at the source plane. Non-dimensional mean flow Mach number, speed of sound, and density $\vec{M}_r, c_r, \rho_r$ are defined relative to reference conditions according to $\vec{M}_r = \vec{V}/c_\infty, c_r = c_l/c_\infty, \rho_r = \rho_l/\rho_\infty$. As noted previously local (dimensional) mean flow velocity, speed of sound, and density are $\vec{V}_0, c_l, \rho_l$. Acoustic perturbations of pressure and particle velocity are also non-dimensional relative to reference conditions according to the replacements $p \to p/\rho_\infty c_\infty^2$, $\vec{v} \to \vec{v}/c_\infty$. Lengths are non-dimensional relative to a reference length R, the duct radius at the source plane, for example $x \to x/R$. Time is non-dimensional according to the replacement $t \to R/c_\infty \, t$. In the time harmonic case, this gives rise to the non-dimensional frequency $\eta_r = \omega R/c_\infty$.

Non-dimensional energy density and intensity are

$$\hat{e} = \frac{e}{\rho_\infty c_\infty^2} = \frac{1}{\rho_r c_r^2} \, p^2 + \frac{1}{2} \rho_r \, \vec{v} \cdot \vec{v} + \frac{1}{c_r^2} (\vec{M}_r \cdot \vec{v}) p \tag{30}$$

and

$$\vec{\hat{N}} = \frac{\vec{N}}{\rho_\infty c_\infty^3} = p\vec{v} + \frac{1}{\rho_r c_r^2} \, \vec{M}_r \, p^2 + \rho_r (\vec{M}_r \cdot \vec{v}) \vec{v} + \frac{1}{c_r^2} \, \vec{M}_r (\vec{M}_r \cdot \vec{v}) p. \tag{31}$$

4. Axi-symmetric ducts

When the duct is axi-symmetric interior power is given by Eq. (28) with the appropriate differential area

$$P_I = \iint_{S_c} \left\langle \vec{N} \cdot \vec{i} \right\rangle r \, \mathrm{d}r \, \mathrm{d}\theta. \tag{32}$$

Time averaging and orthogonality of the angular dependence of the acoustic modes ($\mathrm{e}^{-\mathrm{i}m\theta}$) eliminates the explicit dependence of acoustic power on the circumferential mode number m. If r is considered as non-dimensional (based on the radius R), then Eq. (32) is cast in the non-dimensional form

$$\hat{P}_I = \frac{P_I}{2\pi R^2 \rho_\infty c_\infty^3} = \int_{S_c} \left\langle \vec{\hat{N}} \cdot \vec{i} \right\rangle r \, \mathrm{d}r. \tag{33}$$

The boundary term from Eq. (29), for the axi-symmetric case

$$P_W = \int_\Gamma \left\langle \rho_l V_0 \left(\frac{p}{\rho_l} + \vec{V}_0 \cdot \vec{v} \right) \zeta \right\rangle r \, \mathrm{d}\theta \tag{34}$$

becomes in non-dimensional form

$$\hat{P}_W = \frac{P_w}{2\,\pi\, R^2 \rho_\infty c_\infty^3} = \left\langle \rho_r M_r \left(\frac{p}{\rho_r} + \vec{M}_r \cdot \vec{v} \right) \zeta \right\rangle r_W = -\left\langle \rho_r M_r \phi_t \zeta \right\rangle r_W, \tag{35}$$

where r_W is the local non-dimensional radius of the duct wall (based on R), ζ is the non-dimensional displacement of the impedance surface, and Eq. (15) has been used to obtain the second form. The dissipation term, interpreted as the axial gradient of power, non-dimensional in the same way is

$$\begin{aligned} \frac{\mathrm{d}\hat{P}}{\mathrm{d}x} &= \frac{1}{2\pi R^2 \rho_\infty c_\infty^3} \lim_{\Delta x \to 0} \frac{I_d}{\Delta x} = \lim_{\Delta x \to 0} \frac{1}{\Delta x} \int_{\Delta x} r_b \langle \zeta_\tau^2 \rangle r_w \, \mathrm{d}s \\ &= r_b \langle \zeta_t^2 \rangle r_w \frac{\mathrm{d}s}{\mathrm{d}x} = r_b \langle \zeta_\tau^2 \rangle r_w \sqrt{1 + \left(\frac{\mathrm{d}r_w}{\mathrm{d}x} \right)^2}. \end{aligned} \tag{36}$$

In Eq. (36), $\mathrm{d}s$ is differential arc length along the boundary and $\mathrm{d}r_w/\mathrm{d}x$ is the local slope of the boundary wall.

Eq. (36) provides a method to calculate the change in total acoustic power $\hat{P}_{T_2} - \hat{P}_{T_1}$ over a finite length of lining

$$\hat{P}_{T_2} - \hat{P}_{T_1} = \int_{L_s} r_b \langle \zeta_t^2 \rangle r_w \, \mathrm{d}s. \tag{37}$$

L_s is the length between two evaluations of the total power measured along the lining.

5. Benchmark calculations

In this section, benchmarking of the analysis leading to definition of acoustic power for lined non-uniform ducts is carried out. The approach is two-fold. In the first instance the general development is tested in the case of a uniform circular duct. Very accurate evaluation of acoustic power is available with the use of duct eigenvalue calculations and theoretical conclusions can be tested. For non-uniform ducts with purely reactive linings the requirement of no dissipation of acoustic power, either locally or over some finite length, provides a computational benchmark.

In Ref. [5], the special case of Eq. (29) was derived and benchmarked for a uniform two-dimensional duct. Here, this is done for a uniform circular duct and the conservation law is benchmarked for typical cases. A simple circular duct eigenvalue routine is used to determine the axial wavenumbers based on a finite element discretization. For each axial wavenumber (each mode), the acoustic power is computed according to Eq. (29), with the result broken down into power without the boundary contribution and power including the boundary contribution. Also calculated is the axial gradient of power $\mathrm{d}P_T/\mathrm{d}x$ and the dissipation term of Eq. (27). These should be equal according to the conservation law.

The first case is for non-dimensional frequency $\eta_r = 22.14$, angular mode number $m = 0$. The flow Mach number is $M = -0.489$. The boundary is particularly active for reactive linings, so for this first case the non-dimensional impedence is $Z = 0.001 - \mathrm{i}3.00$. The small resistance is required to help sorting of the axial wavenumbers in the order of attenuation. Table 1 briefly summarizes results of power calculations for the first three cut-on modes (modes 1–3) and the first two cutoff modes (modes 9 and 10) for propagation to the right (designated $+$, decaying to the right) and to the left (designated $-$, decaying to the left). Shown are cut-off ratio, the acoustic power calculated without the boundary contribution, the acoustic power calculated with the boundary contribution, the axial derivative of power calculated from the left-hand side of Eq. (27) and the dissipation, calculated from the right-hand side of Eq. (36). No attempt is made to adjust modal amplitudes to achieve any form of normalization. The first observation is that the gradient of power and dissipation is very

small in all modes, as it should be for a basically reactive lining. Power gradient and dissipation compare almost exactly.

A second observation concerns the contribution of the interior power (without boundary power). Note that for x positive, mode 1 interior power is negative while the total power is positive. Accounting for the boundary power is essential to produce the correct sign for the total power.

Finally, the two cut-off modes for both directions of propagation have significant contributions from the boundary power, and accounting for boundary power is essential in producing the result of nearly vanishing power in these modes. It is interesting to note that mode 1 for positive x and mode 1 for negative x appear to have the same power gradient and dissipation.

The second benchmark case involves the circular duct with $\eta_r = 22.14$, $m = 16$, $M = -0.489$. The impedance is $Z = 3.6-i1.3$. Table 2 shows the results for this case, retaining the two propagating modes and one cutoff mode. The boundary power contribution is not as large as in the purely reactive case, but is not negligible. The power gradient is much larger than in the reactive case as expected because of the resistive part of the impedance, and the comparison with the dissipation is exact to the accuracy retained. An interesting feature here is the presence of two modes for x positive and one for x negative with exactly the same power gradient and dissipation. A similar phenomenon was observed in the first benchmark case.

Another benchmark calculation considers the same case of frequency, angular mode and Mach number described in Table 1, but with a lining of finite length and all eight propagating modes input. The lining length is one-half of the duct radius, $L = 0.5$, extending from $x0 = 0.25$ to $xL = 0.75$. For this reactively lined duct, power is calculated by post-processing FEM calculations of the acoustic field using Eqs. (33) and (35) at six cross-sections, $x1 = 0.302$, $x2 = 0.402$, $x3 = 0.452$, $x4 = 0.552$, $x5 = 0.602$, and $x6 = 0.702$ (multiples of duct radius). Comparison is made with power calculated at the source and termination planes (equal power for this reactive lining) by an alternative approach [10,11] using an eigenfunction expansion and computed axial

Table 1
Benchmark calculations for acoustic power in a uniform circular lined duct determined from acoustic modes and wavenumbers

$\eta_r = 22.14$, $m = 0$, $M = -0.489$, $Z = 0.001-i3.00$

Mode	Cutoff ratio	Power w/o boundary	Power with boundary	dP/dx	Dissipation
1+	113	−0.112−02	0.433−03	−0.222−03	−0.222−03
2+	10.2	0.655−01	0.654−01	−0.433−06	−0.433−06
3+	4.4	0.279−01	0.279−01	−0.974−06	−0.975−06
9+	0.998	0.218−03	0.108−05	−0.435−05	−0.435−05
10+	0.886	0.200−03	0.140−06	−0.427−05	−0.426−05
1−	24700	−0.613+00	−0.636+00	−0.223−03	−0.222−03
2−	8.26	−0.385+00	−0.387+00	−0.176−04	−0.179−04
3−	3.88	−0.183+00	−0.184+00	−0.155−04	−0.156−04
9−	0.998	0.216−03	−0.107−05	−0.434−05	−0.435−05
10−	0.886	0.200−03	−0.140−06	−0.426−05	−0.426−05

Table 2
Benchmark calculations for acoustic power in a uniform circular lined duct determined from acoustic modes and wavenumbers

$\eta_r = 22.14$, $m = 16$, $M = -0.489$, $Z = 3.60-i1.3$

Mode	Cutoff ratio	Power w/o boundary	Power with boundary	dP/dx	Dissipation
1+	1.15	0.556−01	0.536−01	−0.491+00	−0.491+00
2+	1.13	0.638−01	0.618−01	−0.491+00	−0.491+00
3+	0.926	0.116−01	0.109−01	−0.196+00	−0.196+00
1−	1.42	−0.180+00	−0.185+00	−0.491+00	−0.491+00
2−	1.10	−0.116+00	−0.118+00	−0.290+00	−0.290+00
3−	0.941	−0.799−02	−0.987−02	−0.207+00	−0.207+00

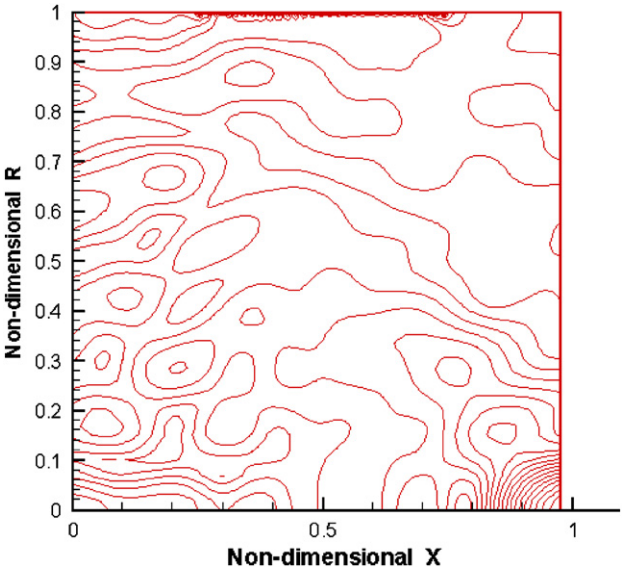

Fig. 2. Acoustic pressure magnitude contours. $\eta_r = 22.14$, $m = 0$, $M = -0.489$, $Z = 0.00-i3.00$. Input is eight propagating radial modes with unit power and random phase. Intense acoustic gradients are clearly evident at the lining.

Table 3
Benchmark calculations for acoustic power at several cross-sections in a uniform circular lined duct obtained by post-processing FEM calculations of the acoustic field

$\eta_r = 22.14$, $m = 0$, $M = -0.489$, $Z = 0.00-i3.00$

x	Power from eig. expansion	Boundary power	Interior power	Total power
$x = 0$	7.884	–	–	–
$x = x1 = 0.302$	–	2.082	5.799	7.881
$x = x2 = 0.402$	–	2.076	5.804	7.881
$x = x3 = 0.452$	–	1.674	6.207	7.881
$x = x4 = 0.552$	–	1.541	6.340	7.881
$x = x5 = 0.602$	–	1.692	6.189	7.881
$x = x6 = 0.702$	–	1.652	6.229	7.881
$x = 0.975$	7.884	–	–	–

wavenumbers. These calculations are very accurate, as no post-processing of FEM results is required. The lining is purely reactive because a small resistance is not required to sort modes in the lined section. The benchmark to be achieved in this case is the verification that to within good accuracy there is no attenuation of acoustic power at any of the chosen cross-sections. In order to achieve the accuracy quoted here, an FEM propagation code based on cubic serendipity elements was used with mesh density doubled in the radial direction near the outer wall.

Fig. 2 shows the acoustic field in the duct when the input is all eight propagating hard-wall modes with unit power and random phase at the source plane $x = 0$. The presence of intense activity at the lined section is evident. The acoustic field at the lining has high gradients and requires an abnormally refined mesh (by the usual standard of 10–15 nodes per wave length). Table 3 shows that power calculated at six interior locations is essentially the same (with allowance for numerical accuracy of post-processing) and compares favorably with power calculated at $x = 0$ and 0.975 (the termination plane). Significant contributions of boundary power are evident, and this depends on location. Total power remains essentially constant. This is required and the numerical results seem to be typical for reactive linings with the level of resolution used here. It should be noted that calculation of acoustic power requires good magnitude and phase resolution of the acoustic field

and is therefore difficult to obtain accurately in the presence of intense acoustic gradients and short effective acoustic wave lengths at the lining. Results obtained in the present case are remarkably good, even though no care was exercised in picking evaluation points (the center of elements at regular intervals along the lining). It is possible to find evaluation points at which the results are more or less accurate than at others, although Table 3 does not show this. Power evaluations given in this example are obtained by post-processing in the interior of elements. In some instances not shown here evaluations have been carried out on the boundaries of elements. Power evaluations on element boundaries are less accurate than in the interior, and are clearly discontinuous across inter-element boundaries (a characteristic of the FEM method as implemented). This is exacerbated in the reactive lining case but tends to disappear if there is only a small amount of dissipation in the lining.

The intense acoustic gradients that appear in the case of Fig. 2 have the appearance of surface waves. The lining impedance in this case is within the range found by Rienstra [13] in which surface waves should be found in lined duct eigenvalue calculations.

A fourth benchmark case considers a non-uniform annular duct with a contraction ratio of 0.7. The benchmark is again confirmation that acoustic power is conserved. The FEM code with cubic serendipity elements again has been used with mesh density doubled near the outer wall. Fig. 3 shows acoustic pressure magnitude contours for the case $\eta_r = 22.14$, $m = 10$. The Mach number at $x = 0$ is $M_I = -0.16$ and the maximum Mach number, which occurs on the outer wall, is $M_{\max} = -0.49$. Lining impedance is again purely reactive with $Z = 0.0-i3.0$. The lining extends from $x = 0.221$ to 0.763. Input is three propagating modes with unit power and random phase. The acoustic field is unremarkable in the entire duct except over the initial upstream section of the lining (the right end of the lining) where intense gradients occur. In this region, it appears that local conditions (particularly flow speed, frequency, Mach number, and impedance) are consistent with the appearance of surface waves. Mesh density used in the computations near the wall was well in excess of the conventional 10–15 nodes per wave length. This case proves to be good for confirming the definition of total power of Eqs. (33) and (35) because there is a region where the boundary contribution to total power is significant and the duct is highly non-uniform. Table 4 provides acoustic power calculations at six points in the lined region as well as at the source and termination (by modal expansion). Interior points are at $x1 = 0.252$, $x2 = 0.402$, $x3 = 0.502$, $x4 = 0.602$, $x5 = 0.702$, and $x6 = 0.748$. These are at element mid-points at regular intervals on the boundary, and were not chosen to place accuracy in a favorable light.

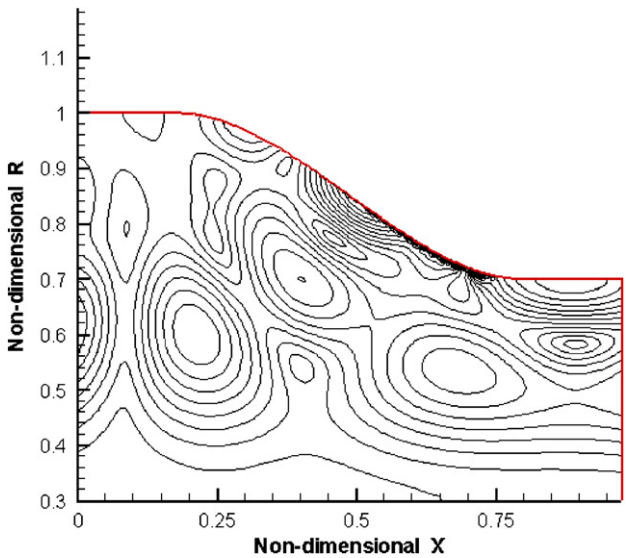

Fig. 3. Acoustic pressure magnitude contours. Non-uniform circular annular duct with cubic polynomial transition. $\eta_r = 22.14$, $m = 10$. Mach number varies from -0.16 to -0.49 along the outer wall. Reactive lining $Z = 0.0-i3.0$. Three propagating radial modes with unit power and random phase.

Table 4
Benchmark calculations for acoustic power at several cross-sections in a non-uniform circular annular lined duct obtained by post-processing FEM calculations of the acoustic field

$\eta_r = 22.14$, $m = 10$, $-0.489 \leqslant M \leqslant -0.16$, $Z = 0.00-\mathrm{i}3.00$

x	Power from eig. expansion	Boundary power	Interior power	Total power
$x = 0$	1.920	–	–	–
$x = x1 = 0.252$	–	−0.036	1.956	1.920
$x = x2 = 0.402$	–	−0.019	1.938	1.920
$x = x3 = 0.502$	–	−0.455	2.376	1.921
$x = x4 = 0.602$	–	−0.490	2.391	1.902
$x = x5 = 0.702$	–	0.080	1.838	1.920
$x = x6 = 0.748$	–	0.372	1.546	1.918
$x = 0.975$	1.920	–	–	–

Table 4 confirms acoustic power conservation from source to termination with allowance made for error associated with post-processing. At all six points in the lined section power remains close to the power at the source and termination ends of the duct, and there is a boundary power contribution with large variation with location. Note that $x4$, $x5$, and $x6$ are in the region of intense gradients at the lining and the maximum error of approximately 1% is observed at $x4$. For the given impedance, frequency, flow speed, random phase choice and mesh density, the high level of accuracy demonstrated is typical outside the area of intense gradients. In the region of intense gradients accuracy can be expected to vary.

6. Dissipative linings

From limited numerical experiments, it appears that resolution of the acoustic field near a reactive lining under certain conditions can be very difficult due to intense acoustic gradients. Only a small amount of resistance in the lining impedance eliminates the intense gradients except possibly right at the transition from hard wall to soft wall. This is shown in the next example. The case of Fig. 3 is retained in every detail except the impedance of the lining, and this is changed to $Z = 0.5-\mathrm{i}3.0$. The acoustic field in Fig. 4 shows considerably reduced activity near the lining.

The benchmark in this case is the change in acoustic power from one point in the lining to another and the comparison of this to the dissipation computed from Eq. (37). Points $x1$ and $x6$ are used, however now $x1 = 0.250$ and $x6 = 0.750$, the left boundary of the first lined element and the right boundary of the last lined element. Power at the source and termination planes is also calculated (by eigenfunction expansion) to set the overall attenuation. The result of the benchmark is shown in Table 5. The calculated dissipation and change in power between $x1$ and $x6$ are very close and compare favorably with the change in power from source plane to termination plane. This serves as a confirmation of the theoretical results.

7. Acoustic radiation

Power calculations described above are equally applicable to ducts radiating to the far field. This provides the opportunity to benchmark power calculations in this application and to determine if conclusions regarding lining performance obtained on the basis of an infinite (non-reflecting) duct model correlate with conclusions obtained based on a model that includes radiation to the far field. There are three features of radiation to the far field that are different from propagation in an infinite duct with similar geometry. The inlet mean flow is not identical in the two cases even though the Mach number at the source plane is identical. The exterior flow in the radiation case plays a role in the details of the interior flow, particularly well upstream of the source plane. For acoustic linings placed near the inlet throat performance may differ. In the radiation code as used here the mean flow field is incompressible with a compressibility correction, while in the propagation code the mean flow is fully compressible. Since power calculations are based on a compressible mean flow, there may be differences in results. Finally, radiation to the far field presents a different impedance to the source than does a

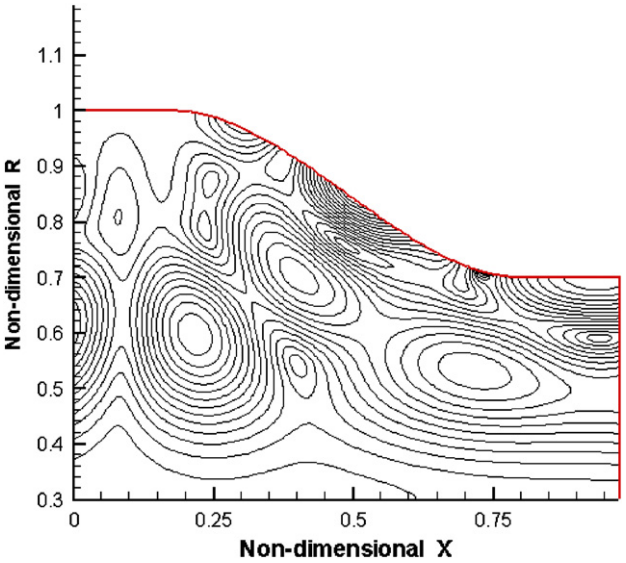

Fig. 4. Acoustic pressure magnitude contours. Annular duct with cubic polynomial transition section $\eta_r = 22.14$, $m = 10$. Mach number varies from -0.16 to -0.49 along the outer wall. Lining impedance is $Z = 0.5-i3.0$. Three propagating radial modes with unit power and random phase.

Table 5
Acoustic power comparisons for duct geometry of Fig. 4

x	Power by eig. expansion	Power from Eqs. (32) and (35)	Dissipation $x1$–$x6$	Delta power $x1$–$x6$
$x = 0$	2.227	–	–	–
$x = x1 = 0.25$	–	2.224	–	–
$x = x6 = 0.75$	–	1.098	1.128	1.126
$x = 0.975$	1.098	–	–	–

reflection free termination, probably altering the details of the acoustic field. These details of the radiation and propagation codes have been discussed in Refs. [9–12].

In the examples considered in this section, calculations have been made with versions of the radiation and propagation codes based on the FEM with cubic interpolation [14,15] on a mesh similar in density to the ones used in previous examples. Cubic interpolation is required to achieve the accuracy for power calculations shown in the following.

The case considered is a turbo-fan inlet geometry shown in Fig. 5. The interior contour has been duplicated up to the throat in an FEM radiation model and in an infinite duct model. Fig. 5 shows sound pressure level contours for the inlet geometry with radiation to the far field. The exterior flow has been set at $M = 0.2$. Other pertinent parameters are shown on the figure. The random phase for the four propagating modes at the source plane is obtained with a random number generator but is the same for both radiation and propagation. An acoustic lining with impedance $Z = 1.0-i1.28$ begins at approximately $x = 0.06$ (relative to the source plane) and extends to approximately $x = 0.75$ in both cases for a lining length of approximately $L = 0.69$. The location is given in approximate terms because the mesh in the two cases is of comparable density but not exactly the same, and lining placement is tied to finite elements and therefore to discrete location possibilities. Lining placement is as near to identical as possible. The impedance was chosen to produce the best attenuation for the random phases chosen. Normalized acoustic power at the source plane is 3.99. Attenuation was calculated with the use of Eq. (32) in the far field. Attenuation achieved was 5.05 dB.

Fig. 6 shows similar results for the reflection free termination model in which only the interior of the duct is modeled. In this case contours are for acoustic pressure magnitude scaled from 0 to 1 on a linear scale. Visual comparison of the acoustic fields of Figs. 5 and 6 reveal considerable similarity, even though the radiation

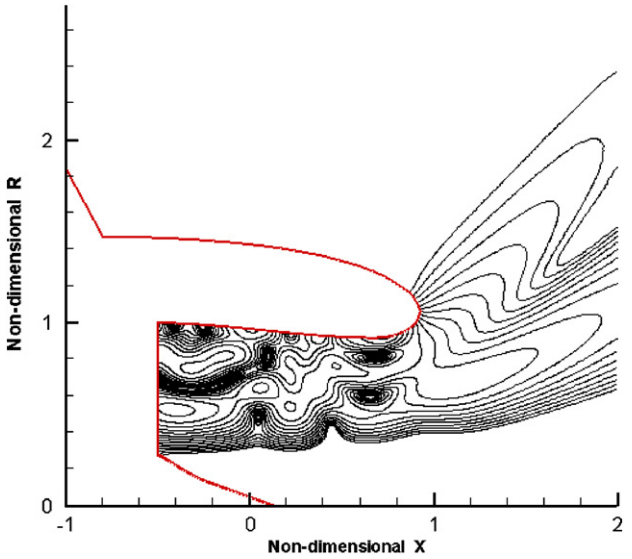

Fig. 5. Sound pressure level contours for FEM radiation model of turbo-fan inlet $\eta_r = 22.14$, $m = 10$. Fan face Mach number $M = 0.49$, Mach number in the far field (forward flight) $M = 0.2$. Lining impedance is $Z = 4.37 - i0.32$. Unit power per mode, random phase.

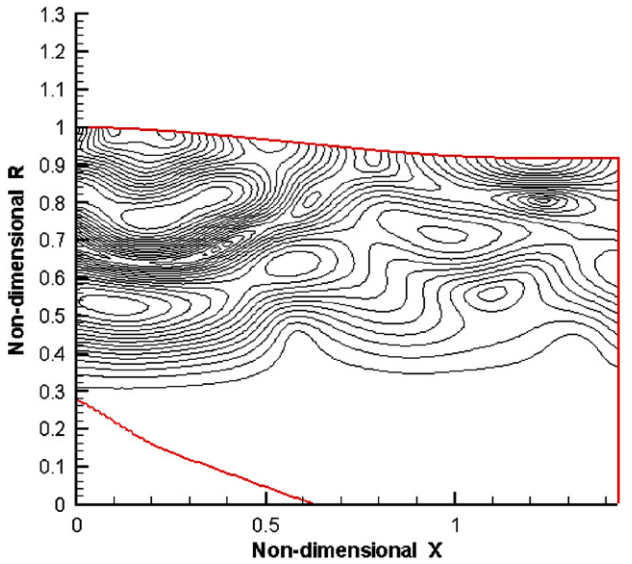

Fig. 6. Acoustic pressure magnitude contours for FEM reflection free termination model for turbo-fan inlet $\eta_r = 22.14$, $m = 10$. Source plane Mach number $M = 0.49$. Lining impedance is $Z = 4.37 - i0.32$. Unit power per mode, random phase.

model contours are SPL, and therefore logarithmically distributed, and the infinite duct contours are simply pressure magnitude, and linearly distributed. For the infinite duct model normalized acoustic power at the source plane is 3.99, and attenuation is 4.98 dB. At least in this case lining performance predicted in the radiation model and the reflection free model is nearly the same. This comparison is exceptionally good, but in other cases may be geometry dependent, particularly when the inlet geometry considerably distorts the flow causing large mean flow gradients in the throat region.

It is interesting to observe the attenuation achieved at set axial positions along the duct and to compare the two cases on this basis. Tables 6 and 7 are used for this purpose. In the case of the radiating duct, power is calculated at $x = 0$ using the accurate eigenfunction expansion, and at $x1 = 0.029$, $x2 = 0.196$, $x3 = 0.304$,

Table 6
Acoustic power comparisons for duct geometry of Fig. 5

x	Power by eig. expansion	Power from Eq. (32)	Dissipation $x1$–$x6$	Delta power $x1$–$x6$	Delta power $x0$–$x7$
$x=0$	3.994	–	–	–	–
$x=x1=0.029$	–	3.993	–	–	–
$x=x2=0.196$	–	3.959	–	–	–
$x=x30.304$	–	3.935	–	–	–
$x=x4=0.401$	–	3.626	–	–	–
$x=x5=0.512$	–	2.507	–	–	–
$x=x6=0.791$	–	1.271	2.722	2.721	–
$x=x7$	–	1.270	(4.972 dB)	(4.971 dB)	2.722 (4.975 dB)

Table 7
Acoustic power comparisons for duct geometry of Fig. 6

x	Power by eig. expansion	Power from Eq. (32)	Dissipation $x1$–$x6$	Delta power $x1$–$x6$
$x=0$	3.994	–	–	–
$x=x1=0.024$	–	3.993	–	–
$x=x2=0.196$	–	3.960	–	–
$x=x3=0.301$	–	3.936	–	–
$x=x4=0.408$	–	3.585	–	–
$x=x5=0.518$	–	2.500	–	–
$x=x6=0.787$	–	1.269	2.721	2.722
$x=L$	1.269	–	(4.972 dB)	(4.971 dB)
			–	2.725 (4.975 dB)

$x4=0.401$, $x5=0.512$, and $x6=0.791$ (multiples of the duct radius) from the source plane. $x1$ is just ahead of the lining. A final calculation is made in the far field at $x=x7$ which is at 2.5 duct radii from the origin shown on Fig. 5 and in the far field. The lining runs from $x=0.056$ to 0.745 from the source plane. In the case of the propagation model, power is calculated at the source plane $x=0$ and the termination plane $x=1.43$ using the eigenfunction expansion and at $x1=0.024$, $x2=0.196$, $x3=0.310$, $x4=0.408$, $x5=0.518$, and $x6=0.787$ measured from the source plane as in the radiating duct. $x1$ is just ahead of the lining and $x6$ is just beyond the lining. The lining runs from $x=0.055$ to 0.747. Tables 6 and 7 show for each location the normalized acoustic power calculated either from the eigenfunction expansion or from Eqs. (33) and (35), as applicable. A first point to note is the comparison between the source side power calculated by eigenfunction expansion and from Eqs. (33) and (35) applied at $x1$ (between the source plane and the lining). With the assumption that the eigenfunction expansion is the baseline, the present theory is judged to produce very accurate results.

Another measure of theoretical consistency and numerical accuracy is the comparison between change in acoustic power (delta power) between two axial positions ($x1$ and $x6$) obtained from Eqs. (33) and (35) and the dissipation calculated from Eq. (37). In both the radiation model and the propagation model this comparison is exceptionally good as noted in columns 4 and 5 in Tables 6 and 7 where the transmission loss based on $x1$ and $x6$, in dB, is also shown.

In the case of radiation to the far-field calculation of power in the far field ($x7$) from Eq. (33) is shown in column 2 of Table 6. The change in power from the source plane to $x7$ is shown in column 6, and compares favorably with delta power and dissipation from $x1$ to $x6$. The small error shown here depends on mesh resolution. Mesh resolution in the far field at the surface denoted by $x7$ is considerably coarser than inside the inlet where all other evaluations are made. A similar comparison is available in Table 7 for the propagation

code. The change in power calculated between source plane and termination plane and the change in power between $x1$ and $x6$ are nearly identical. The conclusion reached is that benchmark calculations for acoustic power for both the propagation code and radiation code are very favorable.

8. Conclusion

Acoustic power is a valuable diagnostic tool for assessment of performance of acoustic treatment in ducts and it also proves to be a valuable metric for the assessment of accuracy of computational codes. A formulation for acoustic power has been extended to lined non-uniform ducts. In lined sections, a boundary power contribution is appended to the classical definition of intensity and power. A conservation law for acoustic power has been obtained and benchmarked using the requirement of power conservation for a purely reactive lining. This proves to be challenging in the case considered because the lining impedance chosen is consistent with the appearance of surface waves and locally reactive behavior near the lining leading to intense acoustic gradients. The boundary power contribution in this instance can be large and both boundary power and interior power may be difficult to compute accurately because of insufficient resolution of the acoustic field. A fundamental result of the power conservation law requiring the change in acoustic power from one duct cross-section to another to be accounted for by the dissipation of the lining is shown to be very accurately predicted numerically. A numerical experiment based on calculation of acoustic power attenuation for a typical turbo-fan inlet modeled with a radiation code and a reflection free propagation code has been used for further confirmation. It has been found that both models predict similar attenuation and comparisons of change in acoustic power and dissipation by the lining in both cases validate the power conservation formulation. Local acoustic power calculations are a valuable tool for assessing lining performance.

Acknowledgment

This research has been funded under a grant from NASA Glenn Research Center.

References

[1] A.D. Pierce, *Acoustics*, McGraw-Hill, New York, 1981.
[2] O.S. Ryshov, G.M. Shefter, On the energy of acoustic waves propagating in a moving medium, *Journal of Applied Mathematics and Mechanics (USSR)* 26 (1962) 1293–1309.
[3] C.L. Morfey, Acoustic energy in non-uniform flows, *Journal of Sound and Vibration* 14 (1971) 159–170.
[4] S.M. Candel, Acoustic conservation principles and an application to plane and modal propagation in nozzles and diffusers, *Journal of Sound and Vibration* 41 (1975) 207–232.
[5] W. Eversman, Acoustic energy in ducts: further observations, *Journal of Sound and Vibration* 62 (2) (1979) 517–532.
[6] W. Moehring, Energy flux in duct flow, *Journal of Sound and Vibration* 18 (1971) 101–109.
[7] O.A. Godin, Reciprocity and energy theorems for waves in a compressible inhomogeneous moving fluid, *Wave Motion* 25 (1997) 143–167.
[8] M.K. Myers, On the acoustic boundary condition in the presence of flow, *Journal of Sound and Vibration* 71 (3) (1980) 429–434.
[9] I. Danda Roy, W. Eversman, Far field calculations for turbofan noise, *AIAA Journal* 39 (12) (2001) 2255–2261.
[10] W. Eversman, The boundary condition at an impedance wall in a non-uniform duct with potential mean flow, *Journal of Sound and Vibration* 246 (1) (2001) 63–69.
[11] W. Eversman, A reverse flow theorem and acoustic reciprocity in compressible potential flow in ducts, *Journal of Sound and Vibration* 246 (1) (2001) 71–95.
[12] W. Eversman, Numerical experiments on acoustic reciprocity in compressible potential flows in ducts, *Journal of Sound and Vibration* 246 (1) (2001) 97–113.
[13] S.W. Rienstra, A classification of duct modes based on surface waves, *Wave Motion* 37 (2) (2003) 119–135.
[14] E. Listerud, W. Eversman, Finite element modeling of acoustics using higher order elements—part I: non-uniform duct propagation, *Journal of Computational Acoustics* 12 (3) (2004) 397–429.
[15] E. Listerud, W. Eversman, Finite element modeling of acoustics using higher order elements—part I: turbo-fan acoustic radiation, *Journal of Computational Acoustics* 12 (3) (2004) 431–446.